Indonesian Physical Review
Volume 07 Issue 02, May 2024
P-ISSN: 2615-1278, E-ISSN: 2614-7904

The Effect of Barium Substitution with Combinations of Rare Earth on Permanent Magnetic Surface Morphology based on Barium Hexaferrite

I Gusti Agung Putra Adnyana[1*], Komang Ngurah Suarbawa[1], Ni Putu Yuni Nurmalasari[1], Wisnu Ari Adi[2]

[1] *Physics department, Faculty Mathematics and Natural Science University of Udayana University, Indonesia.*
[2] *Centre for Science and Technology of Advanced Materials, Tangerang Selatan, Indonesia.*

Corresponding Authors E-mail: igaadnyana@unud.ac.id

Article Info

Article info:
Received: 19-12-2023
Revised: 16-01-2024
Accepted: 05-03-2024

Keywords:
Barium hexaferrite; barium substitution; particle surface morphology

How To Cite:
I. G. A. P. Adnyana, K. N. Suarbawa, N. P. Y. Nurmalasari, W. A. Adi, "The Effect of Barium Substitution with Combinations of Rare Earth on Permanent Magnetic Surface Morphology Based on Barium Hexaferrite," Indonesian Physical Review, vol. 07, no. 02, p 185-193, 2024.

DOI:
https://doi.org/10.29303/ipr.v7i2.300

Abstract

The development of hard magnets today is progressing very rapidly. Developing hard magnets based on rare earth metals becomes a severe problem when the raw materials are not readily available. The chosen solution is to replace oxide-based permanent magnets with small amounts of rare earth metals substituted to improve their magnetic properties. This study synthesized a permanent magnet oxide based on barium hexaferrite doped with lanthanum and cerium atoms. In the synthesis of this material, a mechanical wet milling technique is used to obtain a single-phase permanent magnetic $Ba_{1-\beta-\gamma}La_{\beta}Ce_{\gamma}Fe_{12}O_{19}$ system with composition (β = 0 - 0.5 and γ = 0 - 0.1). The precursors are weighted according to their stoichiometric composition. Each mixed composition was milled by high energy milling (PW 1000 in the mixer/mill) at a milling speed of 1000 rpm using steel balls with an average diameter of 12 mm. Grinding conditions included a ball-to-powder weight ratio of 2:1, milling time 5 hours, then compacted with 7000 Psi pressure and sintered at 1200^{o}C for 2 hours. The surface morphology and microstructure of the resulting sample particles were observed using scanning electron microscopy (SEM) with the SEM JEOL JED 305 brand. The characterization results show that the particles are hexagonally homogeneous in shape with particle sizes in the range of 1000-2000 nm for β = 0 and γ = 0 (without doping). The four samples with varying concentrations of doping ions La^{3+} and Ce^{4+} showed homogeneous hexagonal structures but smaller particle sizes than pure barium hexaferrite. The sample particle sizes ranged from 500-1000 nm for β = 0.02 and 300-1000 nm for β = 0.04.

Copyright © 2024 Authors. All rights reserved.

Introduction

Hard magnets are essential components needed by the automotive industry [1]. Permanent magnets in electric motors must operate at temperatures of 200^{o}C without reducing their magnetic capability [2]. Depending on their constituent materials, there are two types of permanent magnets: metal alloy permanent magnets and ceramic oxide permanent magnets. Both have their advantages and disadvantages. Although metal alloy-based permanent magnets are powerful magnets, this type of magnet is not easy to manufacture, has low corrosion resistance, and has the disadvantages of relatively low operating temperature (Tc = 300^{0}C); it also has small product energy[3].

Rare earth metals are abundant on Indonesian coasts, and the refining process has been mastered [4]. The results of this monazite sand extraction can produce La_2O_3, CeO_2, and Nd_2O_3. This material can be used as an ingredient in making permanent magnets.

Several pieces of literature show that lanthanum substituting strontium and cobalt covering iron has significantly increased hexagonal ferrite's coercivity field and remanent magnetization [2], [5]. Moreover, by reducing the particle size, the coercive field can be almost doubled when the particle size is less than 100 nm[6], [7]. However, this reduction in particle size results in a single domain, which generates a solid, robust dipolar force that opposes the alignment of its magnetic spins under an external magnetic field[8].

Previous research has been conducted to make oxide permanent magnets substituted with La^{3+} ions [9]. The results show that the La^{3+} doped ion barium hexaferrite sample raised the magnetic coercivity field in the composition of $Ba_{0.96}La_{0.04}Fe_{12}O_{19}$ [9]. Subsequent research used Ce^{4+} doping ions, the results identified a single phase at a composition of x = 0.1, while for x > 0.1 a secondary phase was formed [5].

In this paper, the authors have focused on synthesizing M-type barium hexaferrite by substituting La^{3+} ions and tetravalent Ce^{4+} ions and their effect on surface morphology and particle size homogeneity [6], [10]. Adding the concentration of La^{3+} ions and Ce^{4+} tetravalent ions together is a new combination where Lanthanum and Cerium atoms can replace some positions of barium without disturbing the Fe positions [11], [12]. The process used to produce this precursor is wet mechanical milling, which has the advantages of being simple, easy, and inexpensive. Moreover, this method can reduce the precursor's particle size and make the mixture more homogeneous with a relatively short milling time [13]– [15].

Experimental Method

Research on the effect of barium substitution with La^{3+} and Ce^{4+} begins with weighing the main research oxide raw materials, namely $BaCO_3$, Fe_2O_3, La_2O_3, and CeO_2, with compositions adjusted to alter the doping of atoms for variations in the concentration of La^{3+} and Ce^{4+} substitutions needed, and the amount was calculated according to stoichiometric calculations. Each mixed composition was milled by high energy milling (PW 1000 in the mixer/mill) at a milling speed of 1000 rpm using steel balls with an average diameter of 12 mm. Milling conditions included a ball-to-powder weight ratio of 2:1, milling time 5 hours, followed by compaction at 7000 psi and sintering at 1200°C for 2 hours. The surface morphology and microstructure of the sample $Ba_{1-\beta-\gamma}La_{\beta}Ce_{\gamma}Fe_{12}O_{19}$ (β = 0, 0.02, 0.04 and γ = 0, 0.05, 0.1) were observed using scanning electron microscopy (SEM) with the SEM brand JEOL JED 305.

Result and Discussion

The surface morphology and microstructure of the sample $Ba_{1-\beta-\gamma}La_{\beta}Ce_{\gamma}Fe_{12}O_{19}$ (x = 0, 0.02, 0.04 and y = 0, 0.05, 0.1) were observed using SEM presented in Figures 1, 2 and 3. Figure 1 shows the particle microstructure of the pure barium hexaferrite sample ($\beta = 0$ and $\gamma = 0$). The particles were hexagonal with homogeneous particle sizes obtained from SEM photographs in the range of 1000-2000 nm [16], [17]. Particle diffusion resulting from the sintering process at 1200^{o}C for 2 hours produces a homogeneous shape as shown in Figure 1 where the crystallization phase of the material has been achieved.

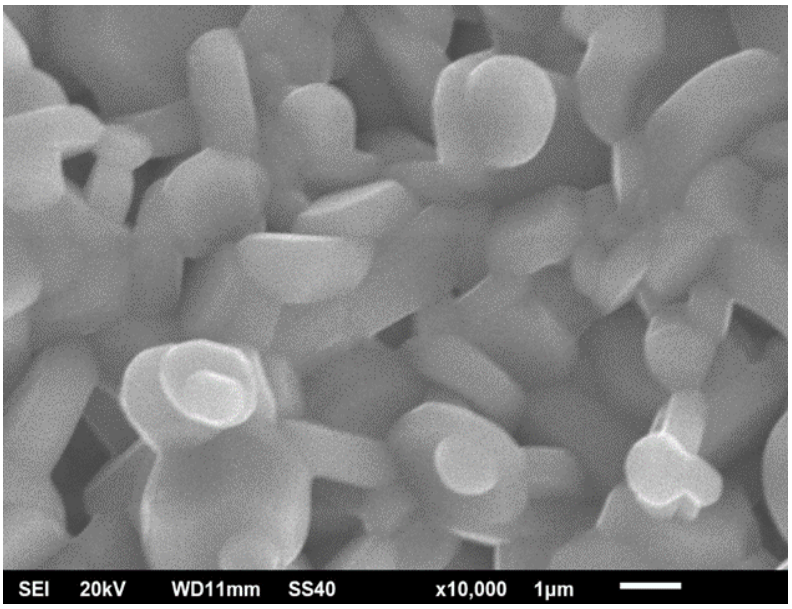

Figure 1. Particle surface morphology of pure barium hexaferrite samples ($\beta = 0$ and $\gamma = 0$)

Figures 2 (a) and 2 (b) showed the surface morphology of barium hexaferrite sample particles doped with La^{3+} and Ce^{4+} ions with compositions $\beta = 0.02$, $\gamma = 0.05$, and $\beta = 0.02$, $\gamma = 0.1$. Based on SEM, the sample particle sizes ranged from 500-1000 nm.

Figures 3 (a) and 4 (b) showed the surface morphology of barium hexaferrite sample particles that have been doped with La^{3+} and Ce^{4+} ions with compositions $\beta = 0.04$, $\gamma = 0.05$ and $\beta = 0.04$, $\gamma = 0.1$.

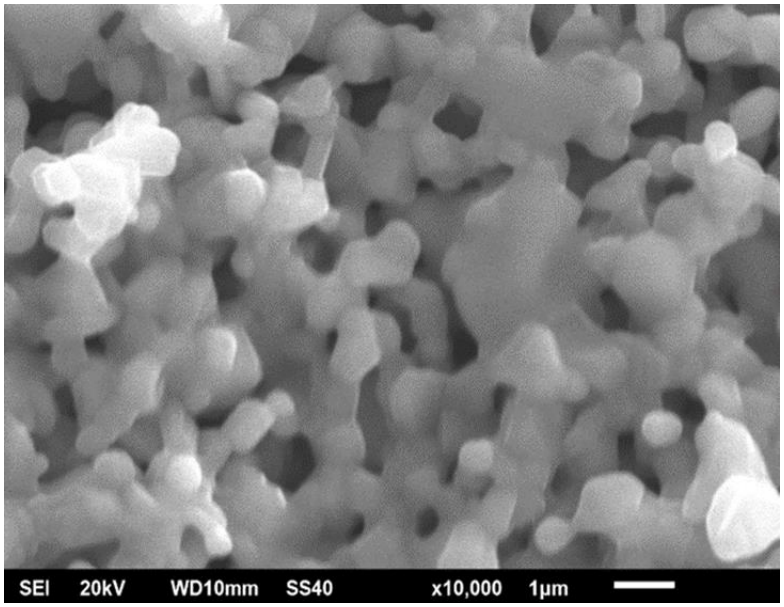

Figure (2a). Surface morphology of barium hexaferrite sample particles doped with La^{3+} and Ce^{4+} ions ($\beta = 0.02$ and $\gamma = 0.05$).

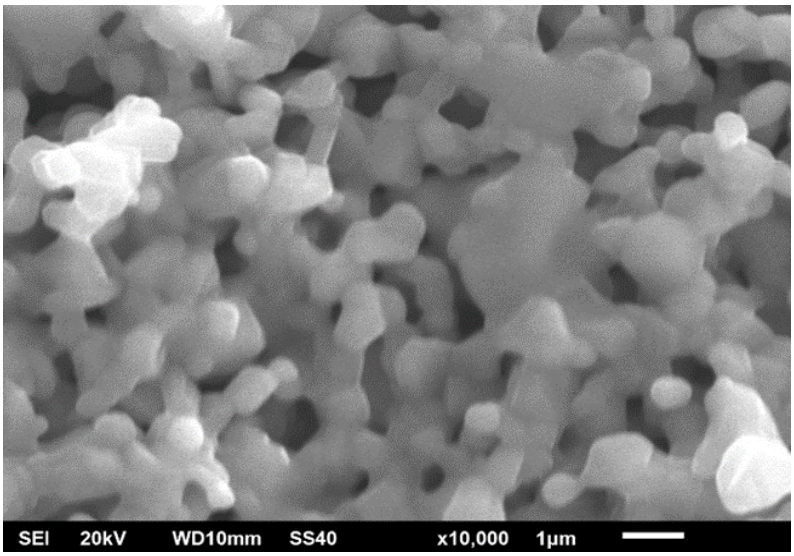

Figure (2b). Surface morphology of barium hexaferrite sample particles doped with La^{3+} and Ce^{4+} ions ($\beta = 0.02$ and $\gamma = 0.1$).

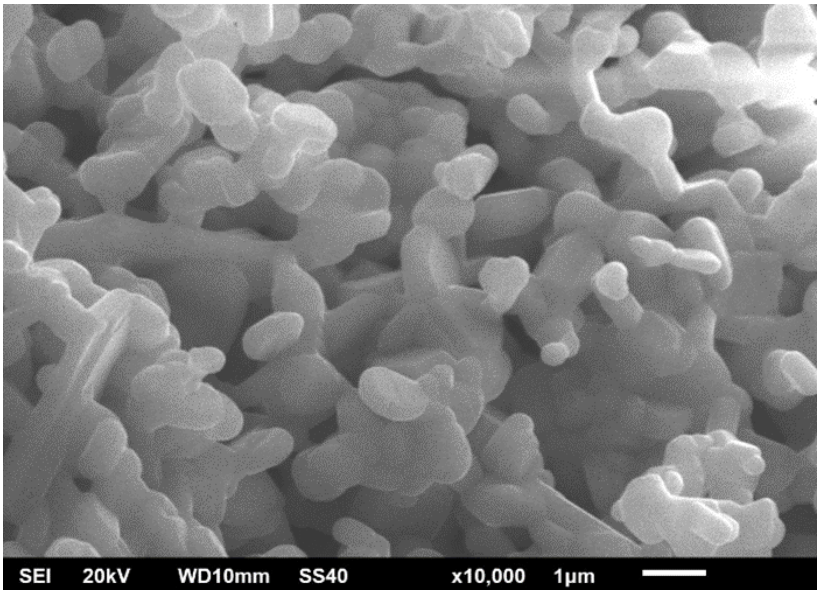

Figure (3a). Surface morphology of sample particles doped with La^{3+} and Ce^{4+} ions ($\beta = 0.04$ and $\gamma = 0.05$)

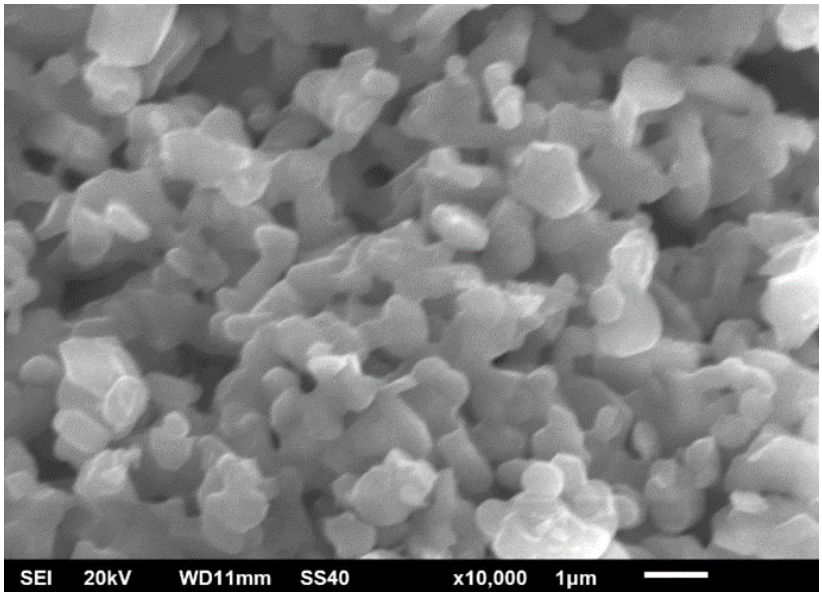

Figure (3b). Surface morphology of sample particles doped with La^{3+} and Ce^{4+} ions ($\beta = 0.04$ and $\gamma = 0.1$).

Based on SEM photos, the particle size from the sample was in the range of 300-1000 nm. Thus, the doping ions La^{3+} and Ce^{4+} played a role in restraining the growth rate of the particles in the sample because they were thought to be related to the high melting temperature of the two doping ions[18], [19]. On the other hand, according to the results of XRD measurements on the Bragg diffraction peaks, slightly doped samples experienced a broadening of the peaks, indicating that the size of the crystallites

was getting smaller so that it had an impact on the formation of the particle size [5], [20]. Unit cell volume data for pure samples is 695.231 $Å^3$, for samples $\beta = 0.02$ and $\gamma = 0.05$ the unit cell volume is 694.686 $Å^3$, and for samples $\beta = 0.04$ and $\gamma = 0.05$ the unit cell volume is 694.241 $Å^3$. Another assumption relates to the doping atomic radius. The doped ionic radius of La (r = 145 pm) and Ce (r = 145 pm) were smaller than the atomic radii of Ba (r = 155 pm). So, the volume of the unit cell also decreases, but it is different from the atomic density, which seems to increase as the doping ion concentration increases. Atomic density data for pure samples is 5.726 g/cm^3, for samples $\beta = 0.02$ and $\gamma = 0.05$ the atomic density is 5.749 g/cm^3, and for samples $\beta = 0.04$ and $\gamma = 0.05$ the atomic density is 5.755 g/cm^3. The overall atomic density was influenced by the density of the doping atoms, which was relatively smaller than the atomic radius of barium, resulting in a decrease in the unit cell volume of this barium hexaferrite crystal[21], [22].

The ion-magnetic cation substitution Ce^{4+} was at the Ba atomic site [14], [23]. The magnetic saturation of samples doped with La^{3+} and Ce^{4+} ions was higher than that of pure barium hexaferrite. Magnetic saturation data for pure samples is 0.28 T, for samples $\beta = 0.02$ and $\gamma = 0.05$ the magnetic saturation is 0.29 T and for samples $\beta = 0.04$ and $\gamma = 0.05$ the magnetic saturation is 0.3 T. The contribution of the non-magnetic doping ion La^{3+} was to restrain grain growth, as indicated by the SEM photo, where the particle sizes before and after doping differed. had sample after doping seemed to have a relatively smaller particle size than before doping. This condition can increase the energy of the domain walls, namely magneto crystalline energy and Zeeman energy, so that it can increase its anisotropic energy[24], [25].

Figure 4 showed that the decrease in particle size in the doped sample was accompanied by a reduction in the crystallite size distribution[26]. The doped ionic radii of La (r = 145 pm) and Ce (r = 145 pm) are smaller than the atomic radius of Ba (r = 155 pm). So, the unit cell volume is reduced. The crystallite size distribution of pure barium hexaferrite samples or samples not doped with La3+ and Ce4+ ions appear larger than that of doped barium hexaferrite samples.

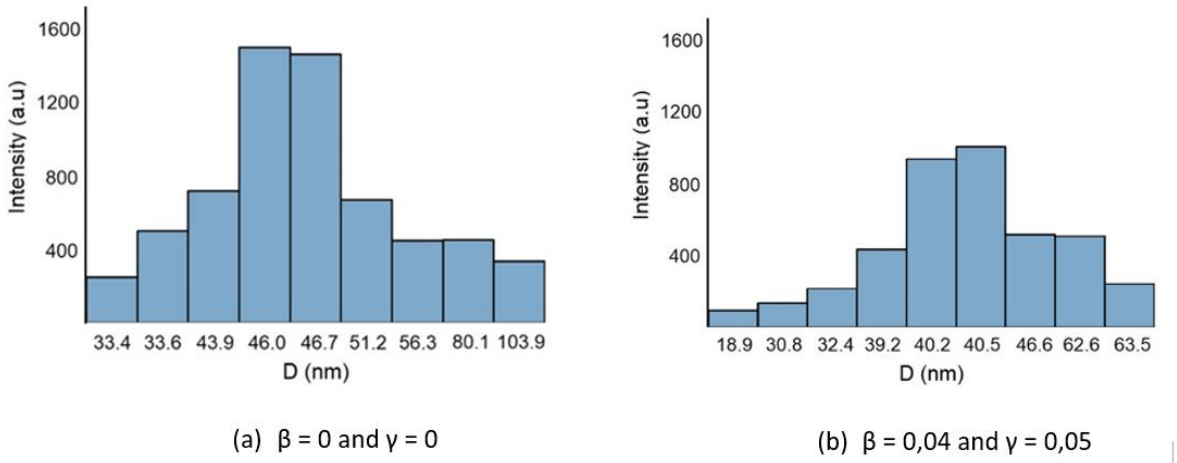

Figure 4. Crystallite size distribution of samples $Ba_{1-\beta-\gamma}La_{\beta}Ce_{\gamma}Fe_{12}O_{19}$; (a) $\beta = 0$ and $\gamma=0$ (b) $\beta=0.04$ and $\gamma =0.05$)

Conclusion

Synthesis of the sample $Ba_{1-\beta-\gamma}La_{\beta}Ce_{\gamma}Fe_{12}O_{19}$ (β = 0.02, 0.04 and γ = 0.05, 0.1) was successfully carried out using the wet mechanical milling method. All samples with varying concentrations of doping ions La^{3+} and Ce^{4+} had homogeneous hexagonal structures but had smaller particle sizes than those of pure barium hexaferrite. Pure samples (β = 0; γ = 0) had particle sizes in the range of 1000-2000 nm, doped samples (β = 0.02; γ = 0.05-0.1) were 500-1000 nm, and doped samples (β = 0.04; γ = 0.05-0.1) were 300-1000 nm.

Acknowledgment

Researchers would like to thank LPPM Udayana University for funding this research.

References

[1] I. G. A. P. Adnyana, I. K. Sukarasa, and K. N. Suarbawa, "Synthesis and characterization of permanent magnetic oxide system $Ba_{1-x-y}La_xCe_yFe_{12}O_{19}$ system doped with La-Ce metal using wet mechanical milling method," *International journal of chemical & material sciences*, vol. 4, no. 1, pp. 43–48, Dec. 2021, doi: 10.21744/ijcms.v4n1.1797.

[2] R. E. El Shater, E. H. El-Ghazzawy, and M. K. El-Nimr, "Study of the sintering temperature and the sintering time period effects on the structural and magnetic properties of M-type hexaferrite $BaFe_{12}O_{19}$," *J Alloys Compd*, vol. 739, pp. 327–334, Mar. 2018, doi: 10.1016/j.jallcom.2017.12.228.

[3] B. D. Chernyshov *et al.*, "A Study of the Microstructure and Magnetic Properties of Fe – Cr – Co Alloys with Reduced Content of Coobtained by the Mim Technology," *Metal Science and Heat Treatment*, vol. 61, no. 11–12, pp. 704–708, Mar. 2020, doi: 10.1007/s11041-020-00486-4.

[4] B. Swain and E. O. Otu, "Competitive extraction of lanthanides by solvent extraction using Cyanex 272: Analysis, classification and mechanism," *Sep Purif Technol*, vol. 83, no. 1, pp. 82–90, Nov. 2011, doi: 10.1016/j.seppur.2011.09.015.

[5] I. G. A. P. Adnyana, I. K. Sukarasa, and W. A. Adi, "Rare earth ion contribution in barium hexaferrite structure to a change of magnetocrystalline anisotropy to improving its magnetic properties," *International Journal of Physical Sciences and Engineering*, pp. 1–13, 2020, doi: 10.29332/ijpse.v4n2.433.

[6] D. A. Vinnik *et al.*, "Morphology and magnetic properties of pressed barium hexaferrite $BaFe_{12}O_{19}$ materials," *J Magn Magn Mater*, vol. 459, pp. 131–135, Aug. 2018, doi: 10.1016/j.jmmm.2017.11.085.

[7] Z. Mosleh, P. Kameli, M. Ranjbar, and H. Salamati, "Effect of annealing temperature on structural and magnetic properties of $BaFe_{12}O_{19}$ hexaferrite nanoparticles," *Ceram Int*, vol. 40, no. 5, pp. 7279–7284, Jun. 2014, doi: 10.1016/j.ceramint.2013.12.068.

[8] J. Liu, P. Liu, X. Zhang, D. Pan, P. Zhang, and M. Zhang, "Synthesis and properties of single domain sphere-shaped barium hexa-ferrite nano powders via an ultrasonic-assisted co-precipitation route," *Ultrason Sonochem*, vol. 23, pp. 46–52, 2015, doi: 10.1016/j.ultsonch.2014.08.001.

[9] I. G. A. P. Adnyana, K. N. Suarbawa, W. A. Adi, N. N. S. K. Wardani, and L. L. S. Jalut, "The effect of lanthanum substitution on the coercivity field in oxide permanent magnet based on $Ba_{1-x}La_xFe_{12}O_{19}$," *International journal of physical sciences and engineering*, vol. 3, no. 1, pp. 42–49, Apr. 2019, doi: 10.29332/ijpse.v3n1.281.

[10] S. Bierlich, F. Gellersen, A. Jacob, and J. Töpfer, "Low-temperature sintering and magnetic properties of Sc- and In-substituted M-type hexagonal barium ferrites for microwave applications," *Mater Res Bull*, vol. 86, pp. 19–23, Feb. 2017, doi: 10.1016/j.materresbull.2016.09.025.

[11] A. Bahadur *et al.*, "Morphological and magnetic properties of $BaFe_{12}O_{19}$ nanoferrite: A promising microwave absorbing material," *Ceram Int*, vol. 43, no. 9, pp. 7346–7350, Jun. 2017, doi: 10.1016/j.ceramint.2017.03.039.

[12] G. F. Liu, Z. D. Zhang, F. Dang, C. B. Cheng, C. X. Hou, and S. Da Liu, "Formation and characterization of magnetic barium ferrite hollow fibers with low coercivity via co-electrospun," *J Magn Magn Mater*, vol. 412, pp. 55–62, Aug. 2016, doi: 10.1016/j.jmmm.2016.03.081.

[13] J. G. Fisher, H. Sun, Y. G. Kook, J. S. Kim, and P. G. Le, "Growth of single crystals of BaFe12O19 by solid state crystal growth," *J Magn Magn Mater*, vol. 416, pp. 384–390, Oct. 2016, doi: 10.1016/j.jmmm.2016.04.079.

[14] I. Haritsah, W. A. Adi, M. V. Purwani, and A. Manaf, "Improved separation of Ce, La, and Nd from a concentrate of rare-earth hydroxide via fractional precipitation," in *IOP Conference Series: Materials Science and Engineering*, Institute of Physics Publishing, Feb. 2019. doi: 10.1088/1757-899X/496/1/012013.

[15] R. Li, S. Pang, C. Ma, and T. Zhang, "Influence of similar atom substitution on glass formation in (La-Ce)-Al-Co bulk metallic glasses," *Acta Mater*, vol. 55, no. 11, pp. 3719–3726, Jun. 2007, doi: 10.1016/j.actamat.2007.02.026.

[16] S. Giri, D. K. Sahu, N. N. Sarkar, and K. G. Rewatkar, "Study of structural and magnetic properties of aluminum-substituted nanosized barium hexaferrite prepared by sol–gel auto-combustion technique," *Bulletin of Materials Science*, vol. 44, no. 2, Jun. 2021, doi: 10.1007/s12034-021-02433-2.

[17] K. Ali, A. K. Sarfraz, I. M. Mirza, A. Bahadur, S. Iqbal, and A. Ul Haq, "Preparation of superparamagnetic maghemite (γ-Fe_2O_3) nanoparticles by wet chemical route and investigation of their magnetic and dielectric properties," *Current Applied Physics*, vol. 15, no. 8, pp. 925–929, Jun. 2015, doi: 10.1016/j.cap.2015.04.030.

[18] V. V. Atuchin *et al.*, "Flux Crystal Growth and the Electronic Structure of $BaFe_{12}O_{19}$ Hexaferrite," *Journal of Physical Chemistry C*, vol. 120, no. 9, pp. 5114–5123, Mar. 2016, doi: 10.1021/acs.jpcc.5b12243.

[19] H. Zheng *et al.*, "Magnetic properties of hexagonal barium ferrite films on Pt/MgO(111) substrates annealed at different temperatures," *J Magn Magn Mater*, vol. 413, pp. 25–29, Sep. 2016, doi: 10.1016/j.jmmm.2016.04.010.

[20] J. Liu, Y. Zeng, X. Zhang, and M. Zhang, "Effects of magnetic pre-alignment of nano-powders on formation of high textured barium hexa-ferrite quasi-single crystals via a magnetic forming and liquid participation sintering route," *J Magn Magn Mater*, vol. 382, pp. 188–192, May 2015, doi: 10.1016/j.jmmm.2015.01.078.

[21] O. Priya, R. K. Singh, S. Bhushan Das, V. Kumar, and S. Farozan, "Optimization of the structural, optical, and magnetic properties of sol-gel derived La^{3+}substituted nanostructured barium hexaferrites," *Phys Scr*, vol. 98, no. 7, Jul. 2023, doi: 10.1088/1402-4896/acd728.

[22] Anju, A. Agarwal, P. Aghamkar, and B. Lal, "Structural and multiferroic properties of barium substituted bismuth ferrite nanocrystallites prepared by sol–gel method," *J Magn Magn Mater*, vol. 426, pp. 800–805, Mar. 2017, doi: 10.1016/j.jmmm.2016.09.103.

[23] X. Song, Y. Wang, C. An, X. Guo, and F. Li, "Dependence of particle morphology and size on the mechanical sensitivity and thermal stability of octahydro-1,3,5,7-tetranitro-1,3,5,7-tetrazocine," *J Hazard Mater*, vol. 159, no. 2–3, pp. 222–229, Nov. 2008, doi: 10.1016/j.jhazmat.2008.02.009.

[24] P. Meng, K. Xiong, K. Ju, S. Li, and G. Xu, "Wideband and enhanced microwave absorption performance of doped barium ferrite," *J Magn Magn Mater*, vol. 385, pp. 407–411, Jul. 2015, doi: 10.1016/j.jmmm.2015.02.059.

[25] P. Gairola, S. P. Gairola, V. Kumar, K. Singh, and S. K. Dhawan, "Barium ferrite and graphite integrated with polyaniline as effective shield against electromagnetic interference," *Synth Met*, vol. 221, pp. 326–331, Nov. 2016, doi: 10.1016/j.synthmet.2016.09.023.

[26] S. Ghaffari, T. Ebadzadeh, M. Alizadeh, K. Asadian, Y. Ganjkhanlou, and M. S. Shafeeyan, "The effects of high-energy ball milling on the synthesis, sintering and microwave dielectric properties of Li_2TiO_3 ceramics," *Journal of Materials Science: Materials in Electronics*, vol. 29, no. 13, pp. 10933–10941, Jul. 2018, doi: 10.1007/s10854-018-9171-4.